Lattice model of gas condensation within nanopores

Raluca A. Trasca, M. Mercedes Calbi, and Milton W. Cole

Department of Physics, Pennsylvania State University, University Park, Pennsylvania 16802
(Received 14 February 2002; published 24 June 2002)

We explore the thermodynamic behavior of gases adsorbed within a nanopore. The theoretical description employs a simple lattice gas model, with two species of site, expected to describe various regimes of adsorption and condensation behavior. The model includes four hypothetical phases: a cylindrical shell phase (S), in which the sites close to the cylindrical wall are occupied, an axial phase (A), in which sites along the cylinder's axis are occupied, a full phase (F), in which all sites are occupied, and an empty phase (E). We obtain exact results at $T=0$ for the phase behavior, which is a function of the interactions present in any specific problem. We obtain the corresponding results at finite T from mean field theory. Finally, we examine the model's predicted phase behavior of some real gases adsorbed in nanopores.

I. INTRODUCTION

A focus of current attention in statistical physics is the behavior of matter in confining geometries [1–12]. An extreme version of this problem arises for adsorption within nanotubes, a case for which the transverse dimensions may be of the order of molecular sizes. One expects an important parameter in this class of problem to be the ratio R^* of the diameter of the molecule to that of the tube. When this ratio is of order 1, the adsorbate may be well described by a one-dimensional (1D) model. As R^* decreases, one expects there to arise successively a sequence of onionlike concentric shells of matter; the number of possible shells is critically dependent on the value of R^*. Accompanying the variation in R^* is a variation of energy scales, which are the crucial variables in the thermodynamics of the system.

Many studies have been performed of specific geometries and specific adsorbate-substrate combinations, as recently reviewed by Gelb *et al.* [13]. However, there have been relatively few studies undertaken of the general problem of adsorption in pores in the case of variable R^*. The present work represents an effort in that direction. Here, we employ a highly oversimplified lattice model of adsorption [14,15] designed for cases when one or two concentric phases of matter (but no more) may be present. Since the present analysis is limited by the assumption of just two distinct species of lattice sites, it describes just the $R^* \geqslant 1$ regime. Hence, there are assumed to be four possible phases for this geometry: an empty phase (E), an axial phase (A), in which atoms are adsorbed only on the cylinder's axis, a cylindrical shell phase (S), in which atoms condense close to the cylinder's wall, and a full phase (F), in which both axial and shell sites are populated with atoms. These are depicted schematically in Fig. 1. We assume a model that includes both pore-site interactions and nearest neighbor interactions. Since the pore attraction is usually different for shell and axial sites, we may think of the axial and shell atoms as two different species interacting with each other with a common value of the chemical potential μ. The same idea was explored in adsorption problems involving two types of binding site [16]. In addition to the pore attraction, the atoms experience an intraspecies interaction (axial-axial or shell-shell) and an interspecies interaction (axial-shell). The phase behavior depends on the values of these various energies, especially on the attractive or repulsive character of the interspecies interaction.

Section II of this paper presents results at zero temperature (T) for the exact phase behavior as a function of the interactions. Section III reports a mean field evaluation of the phase behavior at finite T. The adsorption behavior given by finite T isotherms is compared to the phase diagrams at $T=0$. Section IV describes the relation between the lattice models and some examples of possible realistic situations, i.e., gases adsorbed in carbon nanotubes of various radii. Ultimately, we would like to relate the systems' properties to energy scales present in the real problem. Since these may not be known, it becomes possible in principle to deduce these by comparing experimentally observed phase behavior with that predicted by the model. In view of the approximations inherent in the lattice model, we believe that our results provide a qualitative picture of the expected phase behavior and its evolution with the size ratio R^* mentioned above.

II. ZERO TEMPERATURE ANALYSIS

As a starting point, we consider adsorption in infinite cylindrical pores at $T=0$. The possible phases are described in the Introduction. The cases when the shell-axial interaction is attractive and repulsive are investigated separately. We will illustrate in detail our analysis for the case of an attractive
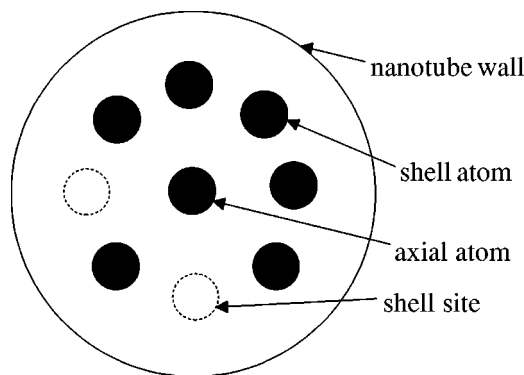

FIG. 1. Schematic transverse section of a nanotube, showing occupied and unoccupied axial and shell sites.

interspecies interaction. Initially, to simplify the discussion, assume that the analysis can be divided into two alternative approaches. In one, we consider the only possible phases to be E, A, and F. In the other, we consider just the phases E, S, and F. We show below that this separation into two distinct treatments encompasses all possibilities for the case of attractive interactions between A and S sites. However, in the case of a repulsive interaction, this division of the problem into two parts does not work, necessitating a somewhat more complicated numerical analysis.

The phase transition diagrams are constructed on the basis of free energy considerations. The shell species is adsorbed on a 2D lattice of sites, with the interaction energy ϵ_s between particles at adjacent sites. For simplicity, this 2D lattice on a cylindrical surface is taken as a square lattice; hence, the number of nearest shell neighbors of a shell atom z_s is 4. The axial species is adsorbed on a 1D lattice of sites, of interaction strength ϵ_a and coordination number $z_a = 2$. We include also the interaction between axial and shell sites, denoted by ϵ_{sa}. Throughout the paper, we express all energies, chemical potentials, and temperatures in units of $\epsilon = \epsilon_s = \epsilon_a$, the absolute value of the interatomic interaction. For simplicity, we assume that shell atoms are positioned on rings whose centers are occupied by axial atoms. The number of axial neighbors for a shell site (z_{sa}) is 1 and the number of shell neighbors for an axial site (z_{as}) is larger than 1.

We first determine the equilibrium phase as a function of μ. The axial, shell, and full grand free energies ($\Omega = F - \mu N$, where F is the Helmholtz free energy) at $T=0$ can be written as

$$\Omega_a = N_a \left(V_a - \frac{z_a}{2} \right) - \mu N_a, \tag{1}$$

$$\Omega_s = N_s \left(V_s - \frac{z_s}{2} \right) - \mu N_s, \tag{2}$$

$$\Omega_f = N_a \left(V_a - \frac{z_a}{2} \right) + N_s \left(V_s - \frac{z_s}{2} \right) + N_s z_{sa} \epsilon_{sa} - \mu (N_a + N_s), \tag{3}$$

where $N_{a(s)}$ is the number of sites in the axial (shell) phase and $V_{a(s)}$ is the interaction potential energy experienced by the axial (shell) site due to the nanotube environment. Adsorption in nanopores at $T=0$ can occur only if the adsorbate is attracted to the interior of the nanopore, i.e., $V_{a(s)} < 0$. We denote the ratio of axial to shell densities (number of atoms per pore length) as $\gamma = N_a / N_s$. The axial and shell cohesive energies per particle are, respectively,

$$E_a = -(V_a - z_a / 2), \tag{4}$$

$$E_s = -(V_s - z_s / 2). \tag{5}$$

These energies consist of the pore attraction energy and the nearest neighbor interaction (the factor of 1/2 avoids double

counting). With this notation, and replacing z_{sa} by 1, the grand free energies can be rewritten as

$$\frac{\Omega_a}{N_s} = -\gamma E_a - \gamma \mu, \tag{6}$$

$$\frac{\Omega_s}{N_s} = -E_s - \mu, \tag{7}$$

$$\frac{\Omega_f}{N_s} = -\gamma E_a - E_s + \epsilon_{sa} - \mu(\gamma + 1). \tag{8}$$

One observes that the adsorption behavior (as a function of μ) depends on four parameters: γ, ϵ_{sa}, E_a, and E_s. The $T=0$ isotherms are determined by finding the minimum of these Ω values and comparing the result with the empty lattice result $\Omega_E = 0$. The axial phase is favored relative to the empty phase if $\Omega_a < 0$, i.e.,

$$\mu > -E_a. \tag{9}$$

The full phase is lower in grand free energy than the empty phase if $\Omega_f < 0$, i.e.,

$$\mu > (-E_s - E_a \gamma + \epsilon_{sa})/(1 + \gamma). \tag{10}$$

The axial phase is favored relative to the full phase if $\Omega_a < \Omega_f$, implying

$$\mu < -E_s + \epsilon_{sa}. \tag{11}$$

An analogous argument is true for the shell phase. $\Omega_s < 0$ implies

$$\mu > -E_s. \tag{12}$$

Note that $\Omega_s < \Omega_f$ if

$$\mu < -E_a + \frac{\epsilon_{sa}}{\gamma}. \tag{13}$$

First, we construct two independent phase diagrams with $E_{a(s)}$ and μ as coordinates, corresponding to the (E,S,F) and (E,A,F) cases. Then, by inspecting the diagrams, we learn how to combine them into a single diagram applicable to both cases at once. We first analyze the E,S,F possible phase transitions alone. The μ regime of each phase is determined by comparison using Eqs. (10), (12), and (13). The transitions between these phases occur at values of μ such that the inequalities (10), (12), and (13) become equalities. In addition, we have to take into consideration that the chemical potential of the pore condensation should be smaller than the chemical potential of bulk condensation in the simple cubic lattice Ising model, which is $\mu_0 = -3$. (Of course, transitions can occur within the pore for $\mu > \mu_0$, but one does not ordinarily study them.) Due to this restriction, we can distinguish two cases. The first occurs when the $S \leftrightarrow F$ transition is below saturation ($-E_a + \epsilon_{sa}/\gamma < -3$). Then all three phases E,S,F are possible, as shown in Fig. 2(a). The alternative scenario occurs when the $S \leftrightarrow F$ transition is above saturation
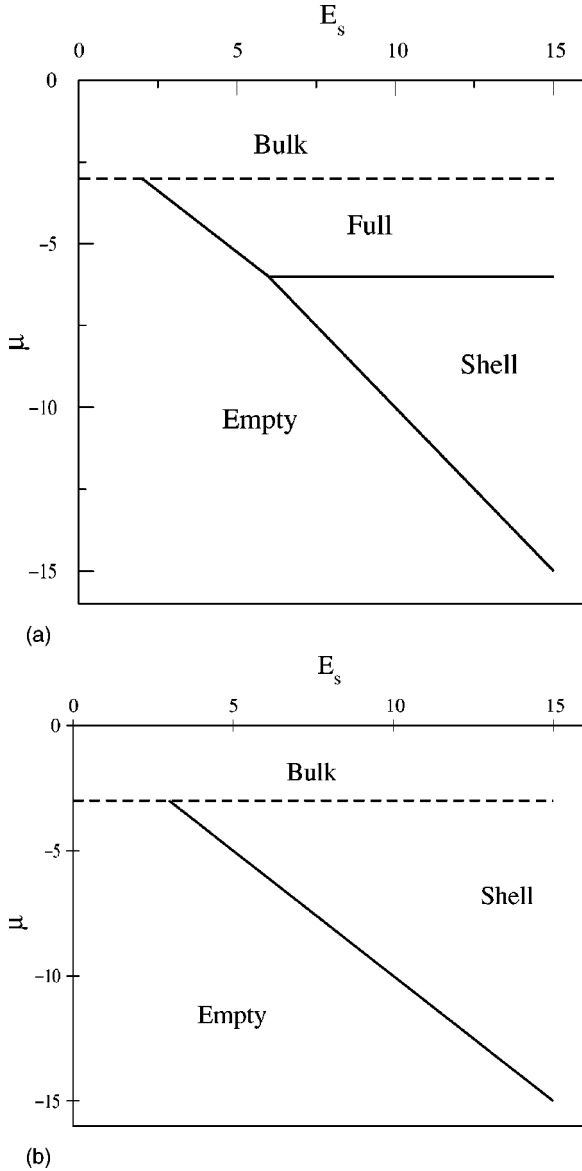
FIG. 2. $T=0$ phase diagram in the case of an attractive axial-shell interaction. μ is the chemical potential and E_s is defined in Eq. (5). Both of these energies are scaled to the intraspecies interaction ϵ. The dashed line is the chemical potential of bulk condensation. We distinguish two cases: (a) when the $S\leftrightarrow F$ transition is present ($-E_a+\epsilon_{sa}/\gamma>-3$) and (b) when the $S\leftrightarrow F$ transition is absent.

$(-E_a+\epsilon_{sa}/\gamma>-3)$. In this case, there are only two possible phases E and S, as shown in Fig. 2(b).

The E,A,F phase analysis is very similar to that above for E,S,F. The two cases that can be distinguished here are (a) $-E_s+\epsilon_{sa}>-3$, when all three phases (E,A,F) are possible and (b) $-E_s+\epsilon_{sa}<-3$, when there are only two possible phases E and A.

So far, the phase transition behavior has been derived from two separate analyses: E,S,F and E,A,F. We now show how the parameter values may be assessed in order to establish which of the two analyses is appropriate to a given system, i.e., a specified set of parameters. To do so, we need to compare values of Ω_a and Ω_s. The difference between
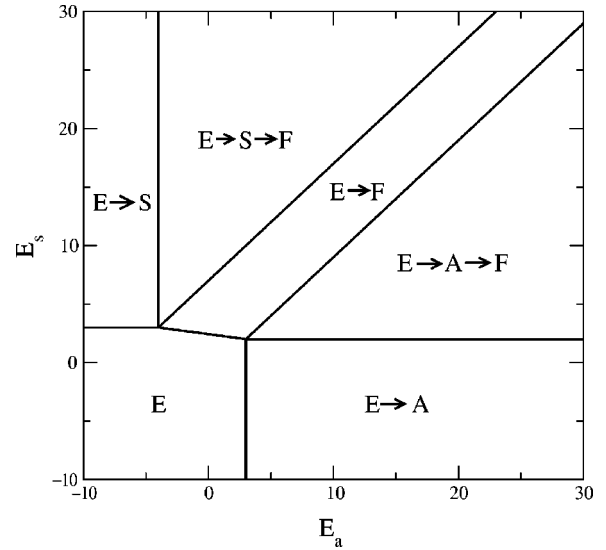

FIG. 3. $T=0$ phase diagram showing the sequence of transitions as a function of shell and axial energies, in the case of an attractive axial-shell interaction. Arrows indicate direction associated with increasing μ.

the relevant free energies satisfies

$$\frac{\Omega_s-\Omega_a}{N_s}=-E_s+E_a\gamma-\mu(1-\gamma).\qquad(14)$$

As can be seen from Eq. (9), the $E\leftrightarrow A$ transition occurs at $\mu_{ea}=-E_a$. In the limit $\mu=\mu_{ea}$, then

$$\frac{\Omega_s-\Omega_a}{N_s}=-(E_s-E_a).\qquad(15)$$

If $E_a<E_s$, then $\Omega_s<\Omega_a$ at this value of μ. At higher values of μ ($>\mu_{ea}$), Ω_s remains less than Ω_a. Hence a transition to the axial phase does not occur for any μ. If, instead, $E_s<E_a$, then $\Omega_a<\Omega_s$ and the axial phase is stable at $\mu=\mu_{ea}$. Is it possible that $\Omega_s-\Omega_a$ changes sign for higher μ (corresponding to an A to S transition)? This would require $\Omega_a=\Omega_s$ at a transition value $\mu=\mu_{as}$ such that

$$\mu_{as}=\frac{E_a(\gamma-\rho)}{1-\gamma},\qquad(16)$$

where $\rho=E_a/E_s<1$. Hence $\rho-\gamma>3(1-\gamma)/E_a>1-\gamma$. This implies $\rho>1$, which violates the assumption $E_s<E_a$. This rules out such a possibility.

The same examination can be done at the $E\leftrightarrow S$ transition line $\mu_{es}=-E_s$; we then find that for $E_s<E_a$, the shell phase does not occur. Hence the possibilities are either $E_s>E_a$ (never the A phase) or $E_a>E_s$ (never the S phase). This justifies the separate analyses used above for the two distinct cases that can arise.

Because the two cases correspond to different regimes of parameter space, $E_s>E_a$ and $E_s<E_a$, they can be merged in a phase diagram that has as coordinates the interactions present in our problem: E_a and E_s. One has only to analyze Figs. 2(a) and 2(b) and find the adsorption sequences as a
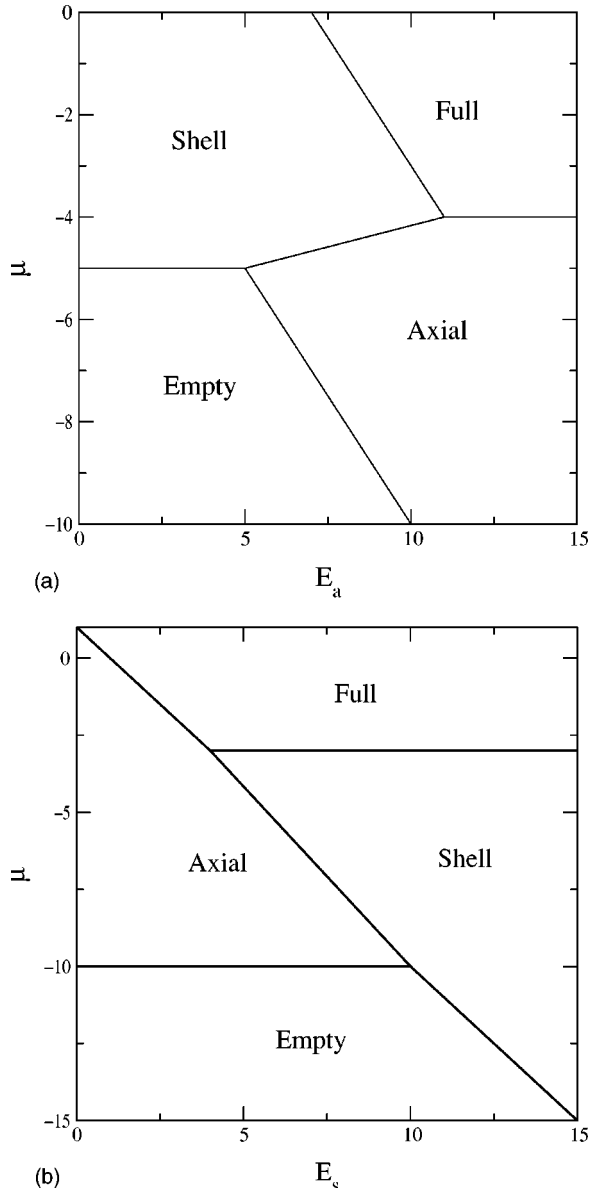
FIG. 4. $T=0$ phase diagram in the case of a repulsive axial-shell interaction (a) as a function of E_s and μ, with E_a fixed and (b) as a function of E_a and μ, with E_s fixed.

FIG. 5. $T=0$ phase diagram of possible transitions as a function of interactions, in the case of a repulsive axial-shell interaction.

function of both interactions when μ is increased. Figure 3 exhibits the regimes of distinct adsorption sequences. All possible sequences occur except those ruled out by the thermodynamic stability condition $\partial\mu/\partial N>0$. The region denoted E corresponds to repulsive, or weakly attractive, pore-gas interactions, so that no atoms adsorb inside the pore. In the $E\rightarrow A$ region, the shell phase's chemical potential of condensation is greater than -3, so the F phase does not occur. Physically, the $E\rightarrow A$ region corresponds to a repulsive, or weakly attractive, pore-shell interaction and an attractive pore-axis interaction; hence, atoms adsorb only at the axial sites. In the $E\rightarrow A\rightarrow F$ region, the attraction in the axial phase is larger than that in the shell phase, so that the axial region is occupied first and then the shell follows at higher μ. Similar reasoning applies to the $E\rightarrow S$ and $E\rightarrow S\rightarrow F$ regions. Possibly the most interesting behavior occurs in the
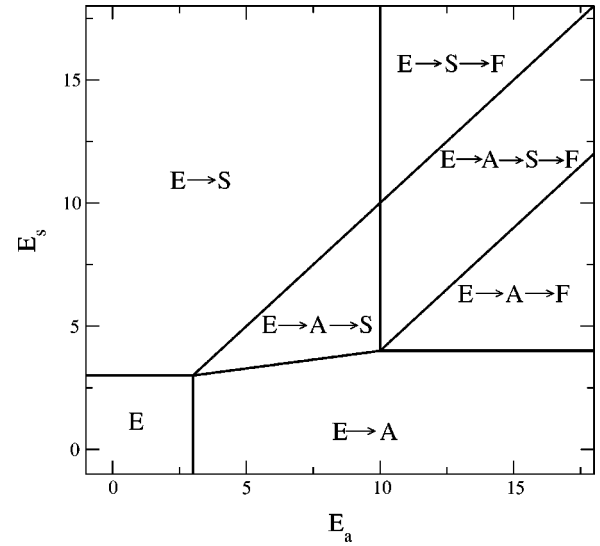
$E\rightarrow F$ region. In general, as seen more clearly at finite T, the axial and shell condensations occur at different chemical potentials. However, in the case of an attractive axial-shell interaction, when the shell and axial energies per particle are similar, the shell and axial phases become cooperative and undergo a common pore filling transition.

We have examined thus far the case of an attractive axial-shell interaction. In the repulsive case, the interspecies interaction energy (ϵ_{sa}) is positive. Then we have to take into account a new possibility, the transition from axial to shell phase (alone). Physically, this means that when the shell atoms are adsorbed, the axial phase, which has a lower density than the shell phase, is expelled by the repulsive axial-shell interaction. Therefore, we compare all the grand free energies $\Omega_a,\Omega_s,\Omega_f$ with each other and the zero energy of the E phase. We present the resulting phase diagrams in (E_a,μ) and (E_s,μ) coordinates in Figs. 4(a) and 4(b). Both diagrams exhibit all phases and possible transitions $E\leftrightarrow A,E\leftrightarrow S,A\leftrightarrow S,A\leftrightarrow F$, and $S\leftrightarrow F$, but there is no $E\leftrightarrow F$ transition. There are several qualitative differences between this case, shown in Fig. 5, and the attractive interaction case, shown in Fig. 3. Missing in the repulsive case is $E\leftrightarrow F$; present in this case are $E\leftrightarrow A\leftrightarrow S\leftrightarrow F$ and $E\leftrightarrow A\leftrightarrow S$ sequences (absent in the attractive case). The last two are associated with the appearance of S, at the expense of A atoms, in order to decrease Ω by adding more particles.

III. FINITE TEMPERATURE ANALYSIS

In this section, we explore the phase transitions at finite T for a gas within our pore. This is a 1D system in the thermodynamic limit of divergent length. To study this model, we use mean field theory. It is known that 1D systems do not exhibit phase transitions at any finite T. However, in the present mean field treatment, we obtain a spurious transition. The results of an exact calculation of the phase behavior in a square pore [17] were found to be *qualitatively* similar to
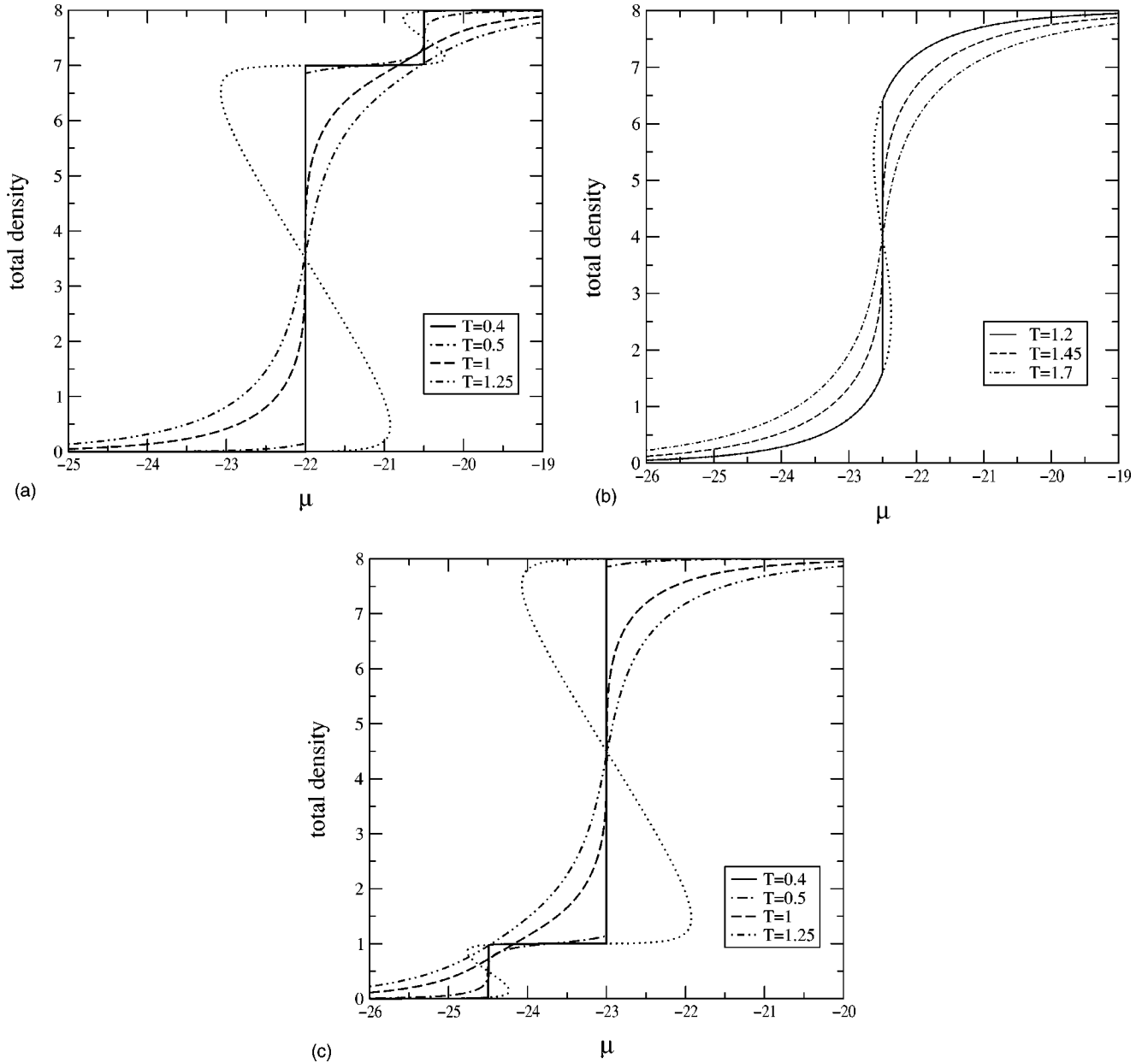
FIG. 6. Adsorption isotherms in the attractive case. In (a) and (c) two transitions $T_{ca}=1$, $T_{ca}=0.5$ (as in the decoupled case) occur for a large difference between axial and shell energies; the phase that is first occupied corresponds to a lower energy, axial for (a), shell for (c). (b) A cooperative transition at a higher T_c occurs when the axial and shell energies are similar.

those of mean field theory, apart from a narrow regime of μ where spurious transitions occur in mean field theory; these are replaced by nearly discontinuous isotherms in the exact case. We note that gases in some nanoporous media (zeolites or nanotube bundles) may represent quasi-1D systems which can go through a genuine phase transition when molecules in adjacent pores are coupled. This transition has been studied recently in a number of models of gases in pores, by both simulations and exact models [18–21].

The occupation probabilities of axial and shell sites are called n_a and n_s, respectively. We construct the grand free energy of the system and minimize it with respect to n_s and n_a. The same procedure was used in Refs. [15] and [22] for analyzing layering and wetting phase transitions. The energy U of the system is a generalization to finite T of the calcula-

tion in Sec. II. Specifically, the energy is

$$U=N_s n_s\left(-\frac{z_s}{2}n_s+V_s\right)+N_a n_a\left(-\frac{z_a}{2}n_a+V_a\right)$$
$$+N_s n_s(z_{sa}n_a\epsilon_{sa}) \tag{17}$$

and the entropy is written as

$$S=-N_s[n_s\ln n_s+(1-n_s)\ln(1-n_s)]$$
$$-N_a[n_a\ln n_a+(1-n_a)\ln(1-n_a)]. \tag{18}$$

The minimization of the grand free energy $U-TS-\mu N$ with respect to the occupation numbers n_a and n_s yields two coupled equations, as found in Ref. [8]:
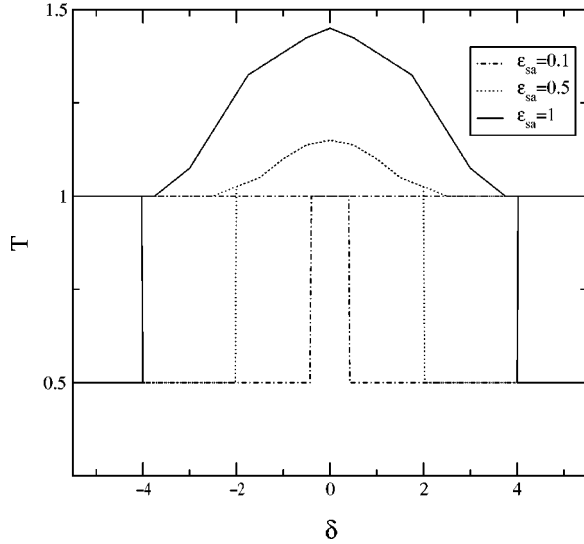
FIG. 7. Dependence of the axial and shell critical temperatures on the difference between axial and shell energies. The two transitions for different μ occurring at large δ merge into one common transition when $|\delta| < 4\epsilon_{sa}$. The width of the cooperative behavior regime is proportional to ϵ_{sa}.

$$n_s = \frac{1}{1 + \exp[-\beta(\mu - V_s - z_s\epsilon_s n_s - z_{sa}\epsilon_{sa}n_a)]},$$

$$n_a = \frac{1}{1 + \exp[-\beta(\mu - V_a - z_a\epsilon_a n_a - z_{as}\epsilon_{sa}n_s)]}. \quad (19)$$

First, we consider the case where the shell-axial interparticle energy $\epsilon_{sa} = 0$, so that we are left with two decoupled Ising problems. It is known that a lattice gas can be regarded as a lattice of spins, with the conversion $s = 2n - 1$, $J = -\epsilon/4$ and the magnetic field $h = (\mu - V)/2 - z\epsilon/4$. One can find the chemical potential of condensation from the condition for the magnetic transition ($h = 0$), and the mean field critical temperature T_c in the Ising model, $\beta_c zJ = 1$, where $\beta_c = (k_B T_c)^{-1}$. In the following, we take Boltzmann's constant $k_B = 1$. Thus, $T_c = z\epsilon/4$. Therefore, in the decoupled case, the shell and axial critical temperatures are $T_{cs} = z_s\epsilon_s/4$ and $T_{ca} = z_a\epsilon_a/4$, respectively. For simplicity, we again use the same axial and shell intraspecies interaction $\epsilon_s = \epsilon_a = \epsilon$, and scale the temperatures with respect to ϵ. Considering a square shell lattice ($z_s = 4$) and a 1D axial lattice ($z_a = 2$), we obtain $T_{cs} = 1$ and $T_{ca} = 0.5$.

Let us consider the effect of turning on the axial-shell interaction. The mean field results are shown in Fig. 6 for $\epsilon_{sa} = 1$. The chemical potential of condensation is found by a Maxwell (equal-area) construction. For a large difference between the energies (per particle) $E_a = -(V_a - z_a/2)$ and $E_s = -(V_s - z_s/2)$, the shell and axial species behave as in the decoupled case; two distinct transitions occur and the transition that occurs first (at lower μ) corresponds to a lower free energy. However, in the case of similar energies, the two species exhibit a common transition. $T_c > 1$ in this case because the cooperative system behaves like a single species of atom, with a larger coordination number.

In order to compare our analysis at finite T with that at $T = 0$, we keep V_s (or E_s) fixed and vary V_a (or E_a), so that we move on a line parallel to the E_a axis. In the finite T case, we watch the resulting evolution of the axial and shell critical transitions. There arises a convenient quantity for characterizing this dependence; this is called δ, defined by

$$\delta = (E_s - \epsilon_{sa}z_{sa}/2) - (E_a - \epsilon_{sa}z_{as}/2). \quad (20)$$

The evolution of these transitions with δ is shown in Fig. 7 for three different interaction strengths. Consider first the strongly attractive case ($\epsilon_{sa} = 1$). For small axial energies per particle ($\delta < -4$), the shell condensation occurs at a lower value of μ than that associated with full condensation. The axial and shell critical temperatures are the same as in the decoupled case (0.5 and 1). This corresponds to the $E \rightarrow S \rightarrow F$ region in Fig. 3. When $\delta = -4$, the effect of interaction between species becomes significant and the two transitions merge. As $|\delta|$ approaches 0, the common transition's critical temperature increases to the value 1.45 (an increase of 45%) at $\delta = 0$. When δ increases from zero to 4, T_c decreases symmetrically with the case $\delta < 0$. This corresponds to the $E \rightarrow F$ region of Fig. 3. A similar critical temperature dependence on the difference between site binding energies was observed in Monte Carlo simulations of benzene condensation in Na-X zeolites [16]. The difference is that, in that case, T_c dropped abruptly to zero when δ exceeded a threshold corresponding to a decoupling of the two transitions (since neither species in that case had an infinite connected path of its own). When $\delta > 4$, the system returns to the case of two separate axial and shell transitions. As the axial-shell attractive interaction is reduced, the range of δ values corresponding to cooperative behavior decreases, as shown in Fig. 7. Note that the maximum value of T_c for the case $\epsilon_{sa} = 0.5$ is only 15% greater than that of the decoupled shell transition. When ϵ_{sa} becomes very small (0.1 in Fig. 7), a single transition occurs for small $|\delta|$, but the transition critical temperature equals that of the shell phase alone.

We have also considered the finite T case of a repulsive interaction, $\epsilon_{sa} < 0$. Again, we study the behavior with E_s constant and vary E_a, so we move on a line parallel to the E_a axis in Fig. 5. The resulting isotherms, corresponding to several different regions in Fig. 5, are shown in Fig. 8. A variety of scenarios can be seen, including those with A either preceding or following S. The behavior as a function of E_s is a logical correlate of that shown in Fig. 5 at $T = 0$. In contrast with the attractive case, there is no $E \rightarrow F$ region, even for similar axial and shell energies, because the shell atoms, which have a higher density, expel the axial atoms. However, a qualitative similarity of the T_c behavior occurs. At low μ, the axial atoms condense first. Then, at higher μ, the shell is occupied while the axis is emptied. This transition occurs at the same T_c as the cooperative transition in the attractive case. When the external pressure (i.e., μ) is sufficiently high to overcome the axial-shell repulsive interaction, a full condensation occurs. These features are expressed in the (T_c, μ) diagram for various values of ϵ_{sa} and $\delta = 0$ (Fig. 9).
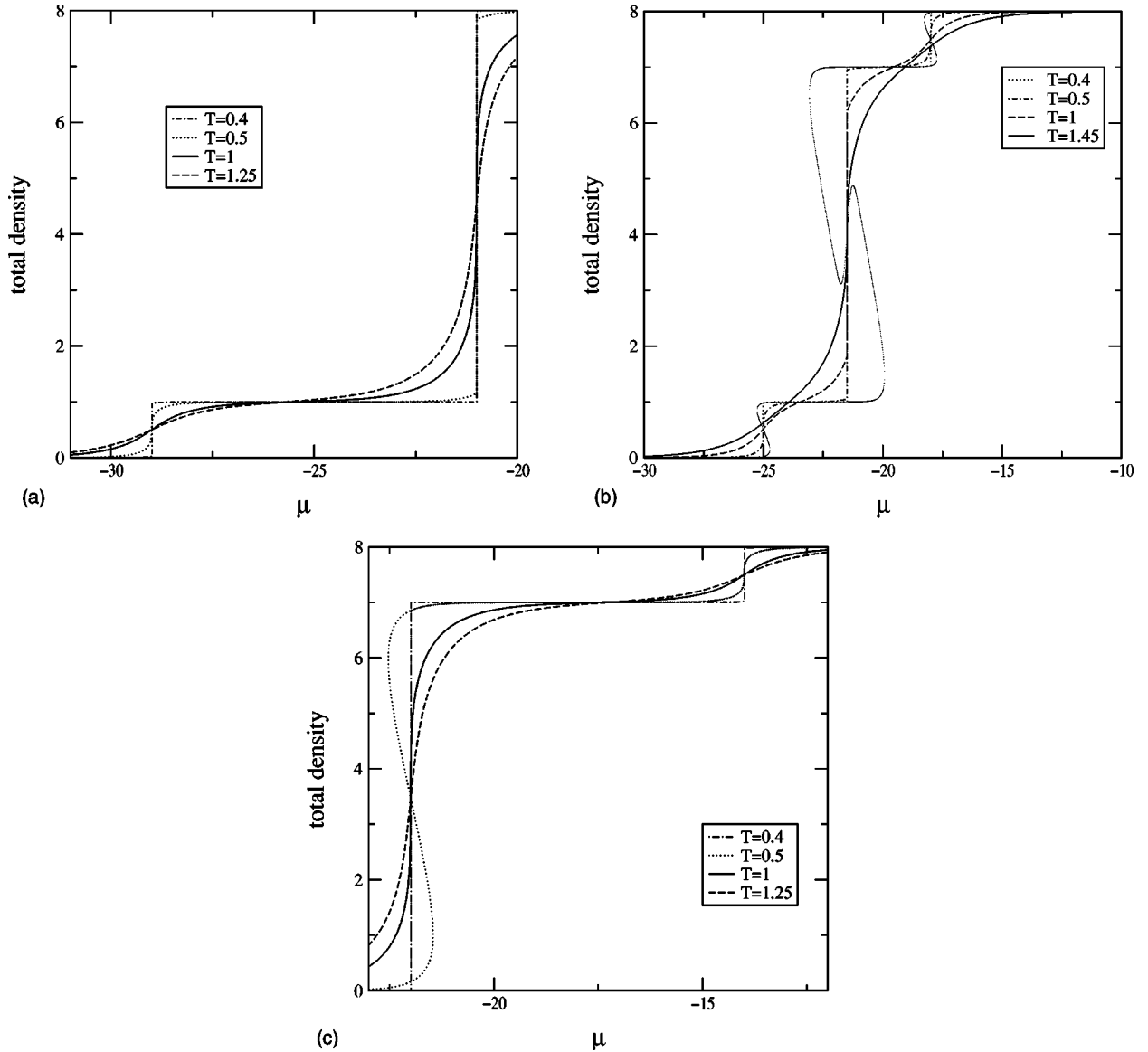
FIG. 8. Isotherms at finite T in the case of repulsive axial-shell interaction. In (a) and (c) two transitions at the decoupled critical temperatures occur for a large difference between the axial and shell energies. The phase that occurs at lower μ corresponds to a lower energy per site. In (b) three different transitions occur when the axial and shell energies are similar.

IV. REAL GASES IN CARBON NANOTUBES

We have discussed so far a simple and general theoretical model for adsorption of gases in a nanopore. Now we consider the model's prediction for a specific case—various gases adsorbed in C nanotubes. In the spirit of the model, we employ a number of simplifying assumptions. The adsorption potential we use is described in [22]; it is a sum of Lennard-Jones (LJ) two-body interactions between the C atoms (spread into continuous matter) and the adsorbate. The energy and distance parameters of this pair potential are obtained from semiempirical combining rules involving the LJ parameters of the C atoms (ϵ_{CC}, σ_{CC}) and the adsorbate (ϵ_{gg}, σ_{gg}) [23–25]:

$$\epsilon_{g\,C} = \sqrt{(\epsilon_{gg}\epsilon_{CC})},$$

$$\sigma_{g\,C} = (\sigma_{gg} + \sigma_{CC})/2. \tag{21}$$

The potential in the nanotube interior at distance r from the axis of the cylinder is [26]

$$V(r,R) = 3\pi\theta\epsilon_{g\,C}\sigma_{g\,C}^2 \left[\frac{21}{32}\left(\frac{\sigma_{g\,C}}{R}\right)^{10} M_{11}\left(\frac{r}{R}\right) \right.$$
$$\left. - \left(\frac{\sigma_{g\,C}}{R}\right)^4 M_5\left(\frac{r}{R}\right) \right], \tag{22}$$

where R is the nanotube radius, $\theta = 0.32$ A^{-2} is the surface density of graphene C atoms, and

$$M_n(x) = \int_0^\pi \frac{d\phi}{[1+x^2-2x\cos(\phi)]^{n/2}}. \tag{23}$$

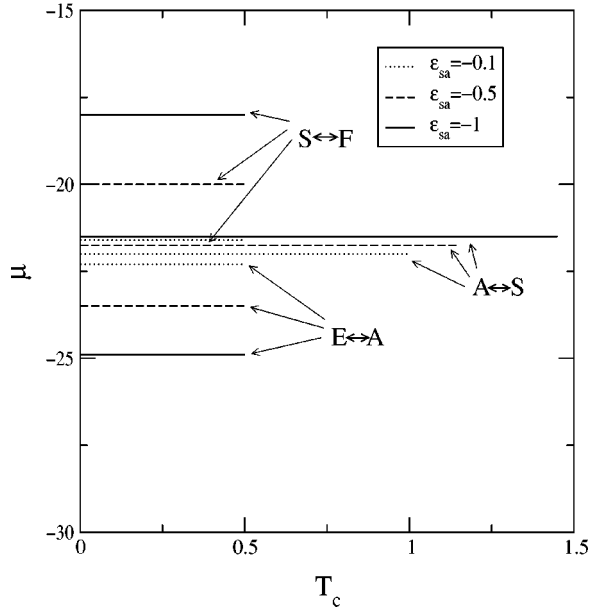The adsorption model is simple: the adatoms condense in a close-packed configuration, in both the shell and axial

FIG. 9. Transition curves in μ-T plane at $\delta=0$ for various values of ϵ_{sa}, in the case of a repulsive axial-shell interaction. The axial sites are filled first; then, when the shell gets filled, axial atoms are expelled and finally, as μ increases, the full phase occurs. As in the attractive case, the critical temperature is enhanced by the coupling.

phases. We are excluding the case of very large R, which would result in the possibility of several concentric shells. As discussed in Secs. II and III, our model has four parameters: the shell and axial energies, the ratio of densities (γ) and the inter-species interaction (ϵ_{sa}). They are not completely independent. One can readily identify the axial potential energy as $V_a = V(0,R)$. To find the shell potential, one should examine the form of the potential. If R is large, $V(r,R)$ has a minimum for a radius R_0 larger than the hard-core adsorbate radius σ_{gg}; then it is logical to assume that the gas atoms will be adsorbed in the shell phase at this distance ($R_s = R_0$) and the shell potential is $V(R_0,R)$. If the pore radius is small ($R_0 < \sigma_{gg}$), it is convenient to identify $R_s = \sigma_{gg}$ and the shell potential $V_s = V(\sigma_{gg},R)$. Geometrical calculations show that this is a good approximation, assuming that shell atoms are positioned near the optimal distance $r_{min} = 2^{1/6}\sigma_{gg}$ from axial atoms. There is arbitrariness in these assignments, a situation that is inherent in any lattice model. V_a and V_s lead easily to the axial and shell energies per particle $E_a = -(V_a - z_a/2)$ and $E_s = -(V_s - z_s/2)$.

The intra- and interspecies interactions are found using Lennard-Jones parameters for the specific gas. The intraspecies interaction energy is taken as ϵ_{gg} and the interspecies energy is the adsorbate-adsorbate interaction at $r = \sqrt{R_s^2 + (r_{min}/2)^2}$:

$$\epsilon_{sa} = 4\epsilon_{gg}\left[\left(\frac{\sigma_{gg}}{r}\right)^{12} - \left(\frac{\sigma_{gg}}{r}\right)^{6}\right]. \quad (24)$$

The number of shell atoms contained in a ring of radius R_s is $2\pi R_s/\sigma_{gg}$ and the corresponding number of axial atoms is 1. Thus, an estimate of the ratio of densities is

TABLE I. Possible transitions for different gases and nanotube radii. The Lennard-Jones parameters are $\sigma_{gg}=3.05$ Å, $\epsilon_{gg} = 37$ K for H_2 and $\sigma_{gg}=4.1$ Å, $\epsilon_{gg}=221$ K for Xe. All interaction energies ($V_s, V_a, E_s, E_a, \epsilon_{sa}$) are expressed in units of the gas hard-core energies ϵ_{gg} and radii in Å. The last column shows the sequence of adsorbed phases as μ increases.

R_{nt}	R_s	V_s	V_a	γ	ϵ_{sa}	E_s	E_a	Sequence
			H_2					
8.0	4.76	-17.3	-2.70	0.10	0.18	19.3	3.70	$E \to S \to F$
7.0	3.75	-18.4	-4.50	0.13	0.54	20.4	5.05	$E \to S \to F$
6.0	3.06	-14.4	-7.35	0.15	0.98	16.4	8.35	$E \to S \to F$
5.9	3.05	-8.92	-8.92	0.16	0.99	10.9	9.92	$E \to F$
5.8	3.05	+1.35	-9.50	0.16	0.99	0.64	10.5	$E \to A$
5.5	3.05	+94.0	-11.7	0.16	0.99	-92.0	12.7	$E \to A$
3.0			+1.74				-0.74	E
			Xe					
8.0	4.20	-10.3	-2.70	0.15	0.95	12.3	3.70	$E \to S \to F$
7.7	4.10	-9.97	-3.14	0.16	0.99	12.0	4.14	$E \to S \to F$
7.6	4.10	-8.91	-3.30	0.16	0.99	10.91	4.30	$E \to F$
7.5	4.10	-7.00	-3.50	0.16	0.99	9.00	4.50	$E \to F$
7.4	4.10	-4.02	-3.67	0.16	0.99	6.02	4.67	$E \to F$
7.3	4.10	+0.18	-3.80	0.16	0.99	1.80	4.80	$E \to A$
7.0	4.10	+39.0	-4.50	0.16	0.99	-37.0	5.50	$E \to A$
4.0			-24.1				25.1	$E \to A$
3.5			-0.50				-1.50	E

$$\gamma = \frac{N_a}{N_s} = \frac{\sigma_{gg}}{2\pi R_s}. \quad (25)$$

Table I presents the resulting values of the various parameters for H_2 and Xe inside nanotubes of various radii. The sequence of transitions is based on the data in Fig. 3. We note several features of these results. First, the only predicted transition scenarios are $E \to S \to F$, $E \to F$, $E \to A$, and no transition. The $E \to S$ and $E \to A \to F$ sequences are not found for H_2 or Xe. Physically, $E \to S$ corresponds to an attractive shell potential (negative V_s) but a repulsive axial potential (positive V_a); and $E \to A \to F$ corresponds to very attractive axial potentials and less attractive shell potentials. These do not occur in our model of nanotubes. We do find $E \to A$ and $E \to S \to F$ transitions for a relatively large range of nanotube radii. The cooperative behavior $E \to F$ occurs for a very small range of parameters because the gas-gas interaction strength is weak in comparison with the nanopore attraction. However, in the case of Xe, which has a much bigger cohesive energy ($\epsilon_{gg}=221$ K) than H_2 ($\epsilon_{gg} = 37$ K), the mutual transition is more common. The H_2 gas undergoes the $E \to S \to F$ transitions for nanotubes with $R > 6$ Å, whereas Xe goes through these transitions only for $R > 7.7$ Å. This is due to the difference between these molecules' sizes and interaction strengths. For $R < 7.3$ Å, Xe can accommodate only the axial phase, whereas the H_2 gas would go into the axial phase for $R < 5.8$ Å. For very small R(3.5 Å for Xe, 3 Å for H_2), gas does not adsorb at all in nanotubes because the pore-gas potential becomes repulsive.

Hartree model calculations and path integral simulations were previously performed for adsorption of H_2 in C nanotubes of radii 6, 7, and 8 Å [27]. Our classical results are in qualitative agreement with these results. The previous study also found the $E \to S \to F$ sequence for this range of nanotube radii. However, their quantum calculations allowed these authors to investigate the delocalization of the axial state. For $R = 8$ Å the axial state's probability density is no longer confined to the immediate vicinity of the axis, exhibiting a maximum near $r = 2$ Å. This is actually not an axial phase, but rather a second shell phase, of small radius. In our calculations, the axial phase is confined to the nanotube axis and such a second shell phase is not considered.

V. SUMMARY AND CONCLUSIONS

We have investigated the adsorption of gases in nanopores, employing a lattice model, which we solved exactly at $T = 0$ and approximately at finite T. Various regimes of transition behavior were found, corresponding to a range of interaction strengths. The sequence of transitions as a function of μ depends on both the axial-shell interaction energy and the difference between the axial and shell energies per particle. When this difference is large, the two species condense independently, i.e., the two species are essentially decoupled. When this difference is small, the behavior depends on the sign of the axial-shell interaction. For $\epsilon_{sa} > 0$ (attractive case), the axial and shell phases undergo a common transition at a higher critical temperature. For $\epsilon_{sa} < 0$, an increase of the critical temperature occurs, corresponding to an $A \to S$ transition.

The most important parameter is the radius of the nanotube or, specifically, the ratio R^* discussed in the Introduction. Even though its value does not appear explicitly in Secs. II and III, it determines most of the other parameters. This is discussed in Sec. IV, where the R dependence of the behavior is explored. Depending on the adsorbate size and interaction strength, we find typically that $E \to A$ occurs for small R^*, $E \to S \to F$ occurs for large R^*, and the coupled condensation ($E \to F$) occurs for a small range of intermediate R^*.

Our approach certainly oversimplifies the real situation in nanopores. First, the lattice gas model constrains the atoms to artificial sites that must be identified only by a very approximate ansatz, discussed in Sec.IV. For light gases, such as H_2 and He, quantum effects (such as zero point motion) are very important, yet they are neglected here. Nevertheless, we think that our model yields the principal qualitative features of the adsorption's dependence on the various interactions present in this problem. Thus it should help us understand the evolution of adsorption phenomena as a function of adsorbate and pore radius.

[1] T. J. Barton, L. M. Bull, W. G. Klemperer, D. A. Loy, B. McEnaney, M. Misono, P. A. Monson, G. Pez, G. W. Scherer, J. C. Vartuli, and O. M. Yaghi, Chem. Mater. **11**, 2633 (1999).

[2] R. A. Guyer and K. R. McCall, Phys. Rev. B **54**, 18 (1996).

[3] V. Talanquer and D. W. Oxtoby, J. Chem. Phys. **114**, 2793 (2001).

[4] K. S. Page and P. A. Monson, Phys. Rev. E **54**, 6557 (1996).

[5] L. Sarkisov and P. A. Monson, Stud. Surf. Sci. Catal. **128**, 21 (2000).

[6] A. J. Liu, D. J. Durian, E. Herbolzheimer, and S. A. Safran, Phys. Rev. Lett. **65**, 1897 (1990).

[7] A. P. Y. Wong and M. H. W. Chan, Phys. Rev. Lett. **65**, 2567 (1990); **70**, 954 (1993).

[8] M. Thommes and G. H. Findenegg, Langmuir **10**, 4270 (1994).

[9] M. Mihayara and K. E. Gubbins, J. Chem. Phys. **106**, 2865 (1997).

[10] M. Schoen, *Computer Simulation of Condensed Phases in Complex Geometries* (Springer-Verlag, Berlin, 1993).

[11] S. Dietrich and M. L. Rosinberg, in *New Approaches to Problems in Liquid Satte Theory*, edited by C. Caccamo *et al.* (Kluwer, Dordrecht, 1999).

[12] R. Evans, in *Fundamentals of Inhomogeneous Fluids*, edited by D. Henderson (Marcel Dekker, New York, 1992).

[13] Lev D. Gelb, K. E. Gubbins, R. Radhakrishnan, and M. Sliwinska-Bartkowiak, Rep. Prog. Phys. **62**, 1573 (1999).

[14] C. Ebner, Phys. Rev. B **28**, 2890 (1983).

[15] M. J. De Oliveira and R. B. Griffiths, Surf. Sci. **71**, 687 (1978).

[16] I. Dukovski, J. Machta, C. Saravanan, and S. M. Auerbach, J. Chem. Phys. **113**, 3697 (2000).

[17] M. R. Swift, E. Cheng, M. W. Cole, and J. R. Banavar, Phys. Rev. B **48**, 3124 (1993).

[18] R. Radhakrishnan and K. E. Gubbins, Phys. Rev. Lett. **79**, 2847 (1997).

[19] M. W. Cole, V. H. Crespi, G. Stan, C. Ebner, J. M. Hartman, S. Moroni, and M. Boninsegni, Phys. Rev. Lett. **84**, 3883 (2000).

[20] M. M. Calbi, F. Toigo, and M. W. Cole, Phys. Rev. Lett. **86**, 5062 (2001).

[21] M. E. Fisher, Phys. Rev. **162**, 480 (1967).

[22] G. Stan, Mary J. Bojan, S. Curtarolo, S. M. Gatica, and M. W. Cole, Phys. Rev. B **62**, 2173 (2000).

[23] W. A. Steele, Chem. Rev. **93**, 2355 (1993).

[24] W. A. Steele, Surf. Sci. **36**, 317 (1973).

[25] G. Scoles, Int. J. Quantum Chem. **24**, 475 (1990).

[26] G. Stan and M. W. Cole, Surf. Sci. **395**, 280 (1998).

[27] S. M. Gatica, G. Stan, M. M. Calbi, J. K. Johnson, and M. W. Cole, J. Low Temp. Phys. **120**, 337 (2000).